IEEE Access
Multidisciplinary | Rapid Review | Open Access Journal

Received 1 September 2022, accepted 22 September 2022, date of publication 3 October 2022, date of current version 10 October 2022.

Digital Object Identifier 10.1109/ACCESS.2022.3211393

RESEARCH ARTICLE

A Low-Profile and Wide-Angle Scanning Planar Ultrawideband Modular Antenna With Ultra-Thin Loading Window

XIN QUAN, ZHENXIN CAO, (Member, IEEE), HUAIMIN ZHOU, AND SHENGCHI ZHU
State Key Laboratory of Millimeter Waves, Southeast University, Nanjing 210096, China

Corresponding author: Zhenxin Cao (caozx@seu.edu.cn)

This work was supported by the National Natural Science Foundation of China under Grant 61471117.

ABSTRACT Ultrawideband phased antenna array has been widely used in communications, radars and detection. However, the high profile and poor wide-angle scanning characteristics have always been the critical limitation for many available ultrawideband antenna applications. In this paper, an ultra-thin loading window (UTLW) is proposed to replace the wide-angle impedance matching (WAIM) superstrate in the planar ultrawideband modular antenna arrays (PUMA), and reduces the profile height greatly. The UTLW consists of two strips in parallel, and each strip is loaded with one resistor and two capacitors. Following the equivalent circuit model (ECM) of the PUMA, the resistance and capacitance are specially designed to make the complex impedance of the UTLW equal to the impedance introduced by the WAIM. A dual-polarized PUMA with an UTLW achieves 6-18 GHz impedance bandwidth with active VSWR $\leq$ 2.6 for scanning up to 60° and active VSWR $\leq$ 3 for scanning up to 70° in E/D/H plane. The profile height of the proposed PUMA is only less than $0.07\boldsymbol{\lambda_l}$, or, $0.24\boldsymbol{\lambda_h}$ with reference to the typical Nyquist half-wavelength spacing frequency. A 20 $\times$ 20 prototype PUMA with the UTLW was fabricated and its measured results were found consistent with the simulation results.

INDEX TERMS Planar ultrawideband modular antenna (PUMA), ultra-thin loading window (UTLW), low-profile, wide-angle scanning.

I. INTRODUCTION

Phased array antennas with wideband, wide-scanning angles, low profile and low cross-polarization have significant advantages in the fields of electronic communications and radars. Obviously, the antenna with wideband, low cross-polarization and wide-scanning angles can achieve remarkably RF/digital hardware reduction and high signal polarization purity. Besides, low-profile antennas have been maturely applied on carried platforms like aircrafts and ships, since they can be in good conformal contact with carrier surfaces.

The traditional wideband Vivaldi antenna achieves over 10:1 impedance bandwidth on broadside in [1] and [2]. However, the extremely high profile and its non-planar structure complicate the integration of Vivaldi antennas and platforms. Furthermore, the wide-scanning performance of Vivaldi antennas are not satisfying [3].

As another typical method to realize wideband, tightly coupled arrays (TCA) have attracted increasing attention with its low profile and wide scanning angles [4], [5]. A tightly coupled dipole array with integrated balun (TCDA-IB) was proposed in [4], whose design shows great potential for expanding the impedance bandwidth and realizing wide-angle scanning. Reference [5] proposed a low-profile TCDA-IB with a novel split ring (SR) instead of wide-angle impedance matching (WAIM) superstrates. The profile height of the array is reduced to $0.063\lambda_l$ or $0.45\lambda_h$ (λ_l/λ_h is the wavelength at the low/high operating frequency). The impedance bandwidth of the array is 0.3-2.15 GHz while scanning up to 70° in E-plane and 45° in H-plane for active VSWR$\leq$3.

The associate editor coordinating the review of this manuscript and approving it for publication was Wanchen Yang.

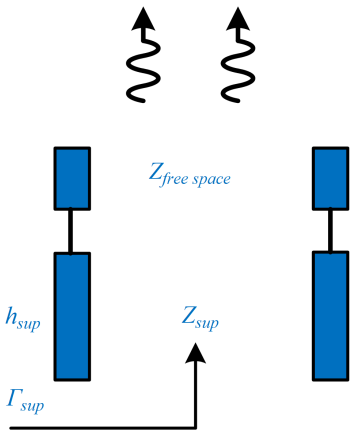

FIGURE 1. Equivalent circuit model of the WAIM.

However, since the linewidth of baluns is hardly affected by frequency under the same characteristic impedance, the baluns of the TCDA-IB are electrically large at higher frequency. In order to reduce the linewidth, the dielectric substrate needs to be thinner, resulting in the instability of the antenna structure [6]. One form of antenna arrays that can work at high frequencies is the connected array [7] which is excited by a simple feed line rather than Marchand balun. A big problem is that the bandwidth of the connected array will be limited by the reflective ground. References [8] and [9] designed an artificial dielectric superstrate which can reduce the distance between the antenna plane and the ground. However, due to the multi-layer structure, the overall profile height is still high. In [10], a low-profile connected slot array with several paralell strips superstrate was proposed. The bandwidth of the connected slot array is 1.35-2.78 GHz with the $0.088\lambda_l$ profile height. But the element distance is only $0.29\lambda_H$, which means a low unit cell gain. References [6], [11], and [12] proposed a new class of planar ultrawideband modular antenna arrays (PUMA). The PUMA consists of a series of tightly coupled dipoles above the ground and is fed by an unbalanced feedline. And it has the merits of low VSWR, wide-scanning angles, low profile as well as modular construction. With a special design for the shorting vias connected to the dipole arms, the PUMA achieves a 6:1 bandwidth with active VSWR ≤ 2 at broadside, VSWR ≤ 3.8 while scanning to 60° in all planes [12].

Another problem is the active impedance mismatching when scanning to a large angle in H-plane. Comparing with matching the change of active impedance in E-plane-scanning, the impedance matching is more difficult to realize in H-plane due to the increasing floquet mode impedance [13]. The TCDA in [5] shows a low active VSWR when scanning within 45° in H-plane, while the active VSWR increases to 4.1 when scanning up to 60° in H-plane. The same conclusion can also be drawn in paper [12], [13], [14], [15]. So far, few papers have offered solution to the problem.

In this paper, a PUMA with ultrawideband, low-profile and wide-angle scanning is proposed. The PUMA has low-profile characteristics due to the ultra-thin loading window (UTLW) which replaces the WAIM. UTLW is designed for thinner thickness while maintain the similar characteristic impedance with WAIM, thus resulting in low profile of the PUMA. The simulation results of the proposed dual-polarized PUMA demonstrate a 3:1 bandwidth for active VSWR$\leq$2 at broadside, active VSWR$\leq$2.6 for scanning up to 60° and active VSWR$\leq$3 for scanning to 70° in the E/D/H plane. The total profile height of the proposed array is $0.07\lambda_l$, or, 0.24 high frequency wavelength with reference to the typical Nyquist half-wavelength spacing frequency.

II. THEORY AND SIMULATION

A. THEORY AND ANALYSIS OF THE UTLW

To analyze the effect of a WAIM on active impedance matching of PUMA, the equivalent circuit model (ECM) of the TCA based on the waveguide theory [16] and Munk's theory [17] is studied in this part. The equivalent characteristic impedance of the free space in Fig. 1 is defined as Z_f, which can be obtained from [18]

$$Z_f = \eta_0 d_E / d_H. \tag{1}$$

η_0 is the wave impedance in free space, d_E is the distance of E-plane element while d_H is the distance of H-plane element. The characteristic impedance of the WAIM Z_{sub} can also be obtained from (1). As shown in Fig. 1, the input impedance obtained by the WAIM transformation of free space impedance can be calculated by

$$Z_{in1} = Z_{sup} \frac{Z_f + jZ_{sup} tan(2\pi h_{sup}/\lambda_{sup})}{Z_{sup} + jZ_f tan(2\pi h_{sup}/\lambda_{sup})}. \tag{2}$$

For replacing WAIM with UTLW, the input impedance should equal as Z_{in1} in (2). Because the thickness of UTLW is thin relative to operating wavelength, the impedance transformation introduced by the dielectric substrate thickness of UTLW can be ignored. The impedance of UTLW is assumed to be Z_x, there is

$$Z_f || Z_x = Z_{in1}. \tag{3}$$

Substitute (2) into (3) and simplify it, and then Z_x can be obtained by

$$Z_x = Z_f/(\sqrt{\varepsilon}_{r1} - 1) + Z_f(\sqrt{\varepsilon_{r1}} - 1)/jtan(2\pi h_{sup}/\lambda_{sup}). \tag{4}$$

where ε_{r1} is the relative permittivity of UTLW dielectric substrate. Equation (4) shows that when h_{sup} is less than $\lambda_h/4$, UTLW has both resistance and capacitance in its complex impedance. For the real part of the Z_x, the value is independent of frequency. For the imaginary part, since the imaginary part of the PUMA input impedance is mainly related to the distance from the antenna plane to the reflective ground [19], the imaginary part of Z_x has little influence. In general, the impedance of the structure same with Z_x theoretically has ultra-wideband characteristics.

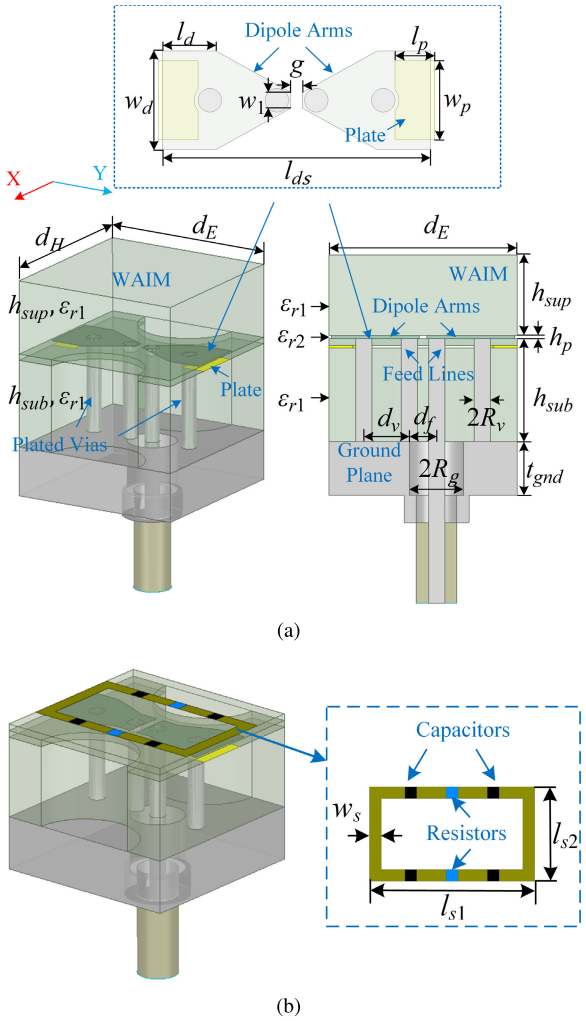

FIGURE 2. Geometry of the single-linear polarized PUMA. (a) Unit cell of the original PUMA with WAIM, the cross section of the original PUMA unit cell and the top view of the radiation patch. The inset is perspective to show the plate. (b) Unit cell of the PUMA with UTLW. The cross section of the PUMA with UTLW is similar with Fig. 2(a). The parameters in Fig.2: $d_E = d_H = 7$ mm, $d_v = 1.7$ mm, $d_f = 1$ mm, $h_{sup} = 3$ mm, $h_{sub} = 3.56$ mm, $h_p = 0.254$ mm, $R_g = 1$ mm, $R_v = 0.3$ mm, $l_{ds} = 6.8$ mm, $l_d = 1.35$ mm, $l_p = 1$ mm, $w_d = 2.5$ mm, $w_p = 2$ mm, $w_1 = 0.4$ mm, $g = 0.3$ mm, $t_{gnd} = 2$ mm, $w_s = 0.5$ mm, $l_{s1} = 7$mm, $l_{s2} = 7$mm. The value of the capacitors is 50 fF and the value of the resistors is 800 Ω.

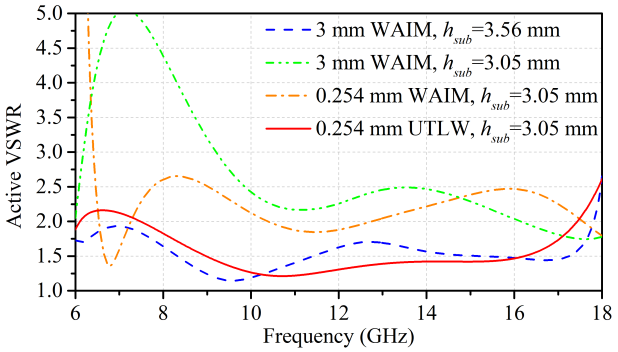

FIGURE 3. Compared of the different active VSWRs between the PUMA with 3 mm WAIM, 0.254 mm WAIM and UTLW. The active VSWR of the original PUMA in Fig. 2(a) is the blue dash line.

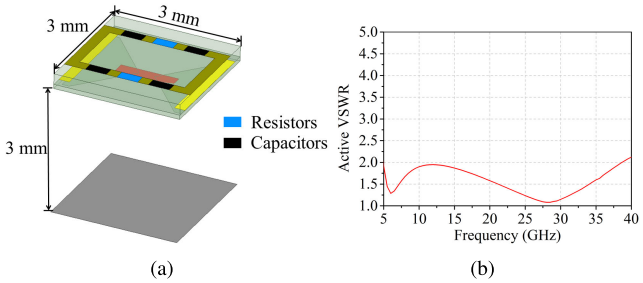

FIGURE 4. Verify of the infinite array with UTLW. (a) The unit cell of the array. (b) Simulated broadside active VSWR of the array.

B. DESIGN OF A SINGLE-POLARIZED PUMA WITH UTLW

A single-polarized PUMA employed from [12] is taken as an example for simulation verification. The original structure of the PUMA antenna cell is shown in Fig. 2(a), and the thickness of WAIM is 3 mm. The relevant dimensions shown in Fig. 2 are optimized by the electromagnetic simulation software HFSS. In the calculation, the master-slave boundary conditions are used to simulate equivalent infinite array. As shown in Fig. 3, the active VSWR of the original PUMA is less than 2.5 in 6-18 GHz frequency band.

In order to reduce the thickness of superstrate, the UTLW is designed according to the results obtained from (4). The structure and the optimized parameters of the UTLW are shown in Fig. 2(b). The UTLW is printed on the other side of the dielectric substrate ($\varepsilon_r = 1.96$) directly above the dipole. The long side of the UTLW are arranged along the main polarization direction of the dipole. Four capacitors and two resistors are loaded on the strip to provide complex impedance. As can be seen from Fig. 3, the PUMA has both low-profile and excellent impedance matching characteristics after loading the UTLW. For comparison, we adjusted the original PUMA with WAIM to the same profile height ($h_{sup} = 0.254$ mm, $h_{sub} = 3.05$ mm). As shown in Fig. 3, the PUMA will be mismatched in the entire operating band when the profile height is reduced without any special designs.

It should be pointed out that the UTLW has the potential to be applied to wider bandwidth antenna arrays, and the 3:1 bandwidth in this paper is not the limitation of the proposed UTLW. It has been analyzed above that the real part of the impedance loaded with UTLW is not related to the frequency, so theoretically UTLW can be applied to wider bandwidth antennas. The bandwidth of the antenna in this paper is 3:1 because it is designed based on a traditional PUMA, which is fed by a simple feed line. The antenna plane and the feed line can excite common mode resonance and loop resonance [11]. Both resonances limit the bandwidth of the antenna. In the follow-up study, the authors found that UTLW can achieve at least 8:1 bandwidths. The results in Fig. 4 proves that the proposed UTLW has the potential of wider operating bandwidth. The infinite antenna in Fig. 4(a) is excited by

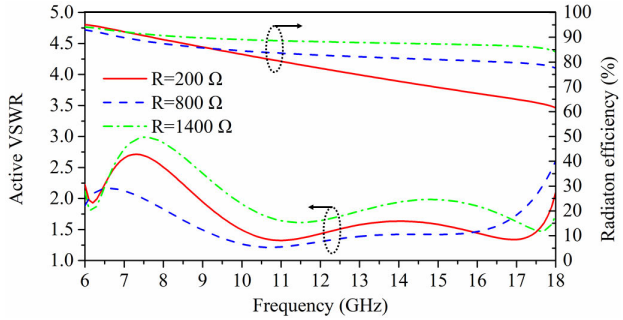

FIGURE 5. Compared broadside radiation efficiency and active VSWR when PUMA loading different value of resistors.

TABLE 1. Broadside radiation efficiency and active VSWR with different resistors.

		Frequency			Active VSWR
		6 GHz	12 GHz	18 GHz	
Resistors	200	94.7%	77.3%	60.5%	≤ 2.7
	400	92.7%	76.7%	67.1%	≤ 2.5
	600	92.5%	80%	72.8%	≤ 2.65
	800	92.8%	82.4%	76.8%	≤ 2.6
	1000	93.2%	84.7%	78.6%	≤ 2.8
	1200	93.9%	86.7%	80.6%	≤ 3
	1400	94%	88.2%	85%	≤ 3.1
	2000	95.4%	90.9%	85.1%	≤ 3.35

the ideal port, so the common mode resonance and loop resonance will not be excited.

The broadside radiation efficiency of the PUMA in Fig. 2(b) after loading resistors with different impedance values is shown in Fig. 5. It can be seen that the broadside radiation efficiency increases when the value of resistance gets larger. The inverse correlation between the broadside radiation efficiency and the resistance is due to the parallel connection of the loading resistance and the radiation resistance. The radiation efficiency can be obtained from equation (5):

$$\xi = 1 - \frac{R_r}{R_L + R_r + jX(f)}, \tag{5}$$

where R_L is the value of the loaded resistor, R_r is the radiation impedance and $X(f)$ is the reactance part of the antenna's impedance which includes equivalent capacitance between antenna elements, reactance introduced from the ground, the reactance introduced by the radiation patch and the reactance introduced by the UTLW. Since the resistance value is related to the active impedance matching, it is necessary to make a trade-off between the broadside radiation efficiency and impedance matching. More detailed broadside radiation efficiency and active VSWR corresponding to different resistance values are listed in Table 1. 800 Ω is selected as the optimal impedance value in the UTLW, and the corresponding radiation efficiency is more than 76%. Compared with the resistance, the capacitance has a little influence on the impedance matching due to the equivalent series capacitance introduced by the strips of the UTLW. On the other hand,

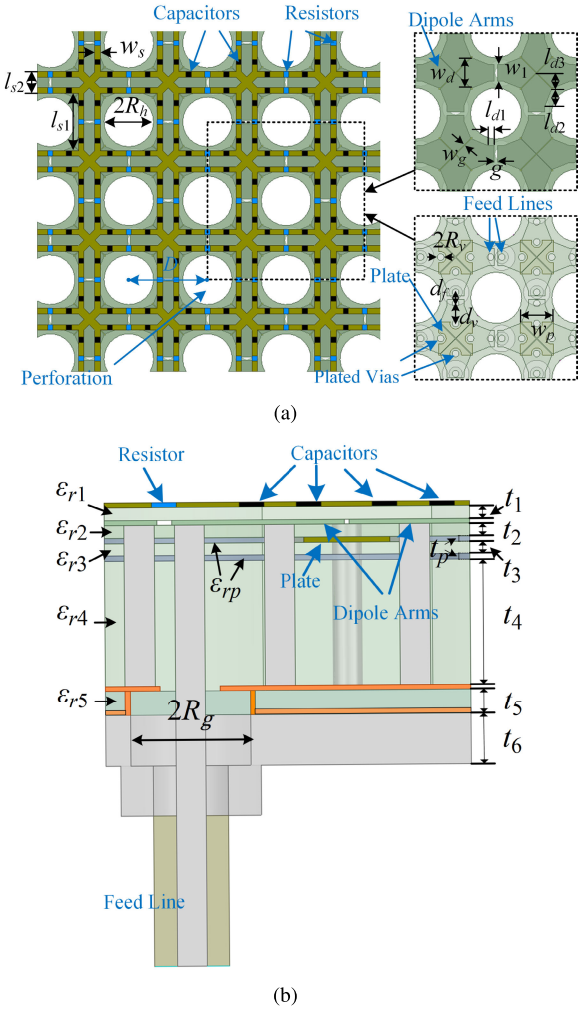

FIGURE 6. Geometry of the dual-linear polarized PUMA with UTLW. (a) Top view of the PUMA. (b) The cross section of the PUMA unit cell. The prepreg layers between the adjacent PCBs are shown in the inset. The parameters in Fig. 6: d_E=d_H = 7.3 mm, d_v = 1.8 mm, R_h = 2.3 mm, R_g = 1.2 mm, l_{s1} = 4.3 mm, l_{s2} = 3 mm, l_{d1} = 0.5 mm, l_{d2} = 1.5 mm, l_{d3} = 1.45 mm, w_s = 0.5 mm, w_d = 2.7 mm, w_p = 3 mm, w_g = 0.05 mm, w_1 = 0.5 mm.

the imaginary part of the antenna input impedance is mainly affected by the distance between the reflecting ground and antenna plane. Therefore, although the capacitance value selected here is 50 fF, it does not mean that other capacitance values are inappropriate.

C. DESIGN OF A DUAL-POLARIZED PUMA

In the previous part, an UTLW structure which can reduce the antenna profile height is designed and applied to a single polarization PUMA. This part will design the UTLW on the dual-polarization PUMA.

The detailed structure of the dual-polarization PUMA loaded with the UTLW is shown in Fig. 6. The UTLW is printed on Rogers 5880LZ (ε_r = 1.96) with a thickness of 10 mil. A series of perforations in the superstrate and

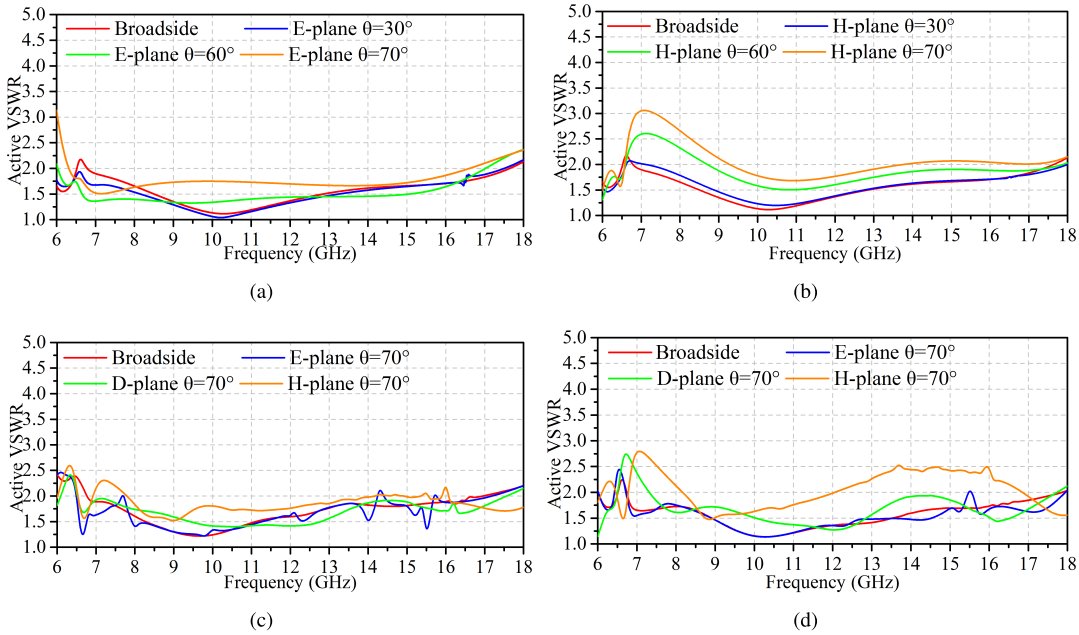

FIGURE 7. Simulated active VSWR of the infinite and semifinite dual-polarized PUMA with UTLW. (a) Scanning in E-plane of the infinite array. (b) Scanning in H-plane of the infinite array. (c) The active VSWR of the edge element in the semifinite array. (d) The active VSWR of the center element in the semifinite array.

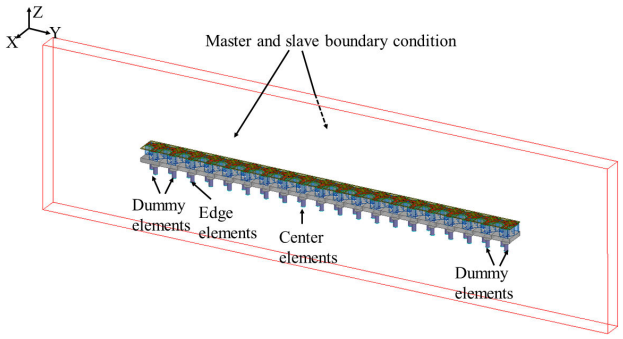

FIGURE 8. The boundary condition of the semifinite dual-polarized PUMA.

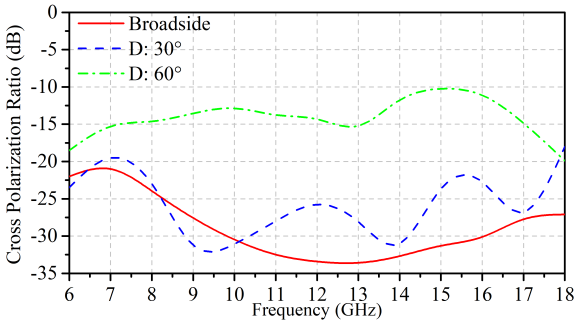

FIGURE 9. Simulated cross-polarization ratio of the PUMA with UTLW when scanning in D-plane.

substrate with the radius $R_h = 2.3$ mm are added for avoiding "scan blindnesses" [6]. The distance of the short vias is optimized to suppress the common mode resonance in the operating frequency band.

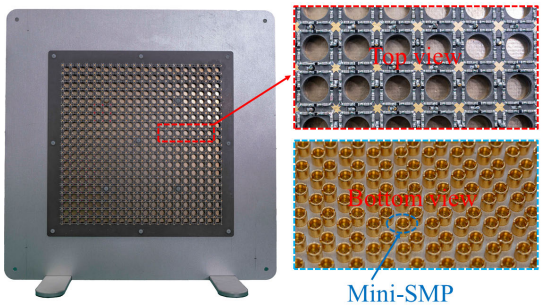

FIGURE 10. Prototype of the dual-linear polarization PUMA with UTLW.

Fig. 7 (a)(b) demonstrate the active VSWR of the infinite dual-polarized PUAM loaded with UTLW. It can be seen that the active VSWR is less than 2.4 in E-plane when scanning to 60° and less than 3 when scanning up to 70° in the frequency band of 6-18 GHz. In H-plane, the active VSWR is less than 2.6 when scanning to 60° and less than 3 when scanning up to 70°. Furthermore, the active VSWRs of the edge element and the center element in the $20 \times \infty$ (the center 16 elements are excited) array when scanning in E/D/H plane are shown in Fig. 7(c)(d). The boundary conditions of the semifinite array are set as shown in Fig. 8. Both ends of the array direction are set as the radiation boundary, and the infinite array direction is set as the master-slave boundary. The four dummy elements on the two edges of the array weaken the influence of the edge effect well.

The cross-polarization ratio is defined as G_{cross}(dB)-G_{co}(dB) and shown in Fig. 9 when scanning to 0°, 30°, 60° in D-plane respectively. In all planes, the

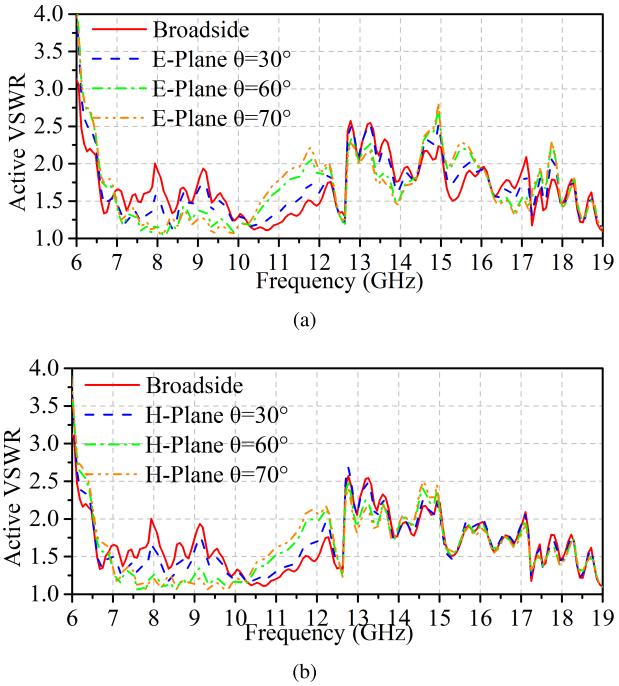

FIGURE 11. Measured active VSWR of the dual-linear polarization PUMA prototype. (a) Scanning in E-plane. (b) Scanning in H-plane.

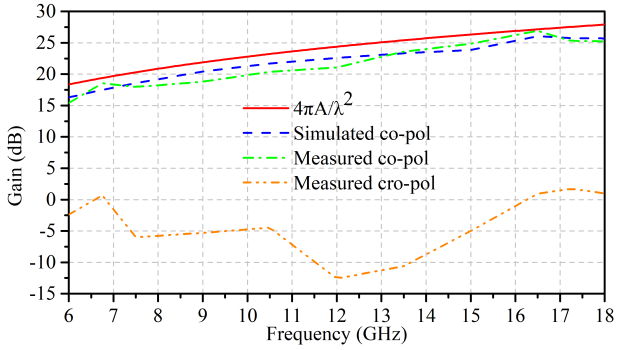

FIGURE 12. Measured and simulated broadside realized gain of the 16 × 16 PUMA with UTLW.

cross-polarization ratio deteriorates the most when scanning in D-plane, so the D-plane cross-polarization ratio can represent the overall polarization purity. As seen in Fig. 9, the diagonal plane results demonstrate satisfying cross-polarization ratio, which is lower than −10 dB at 60°.

III. FABRICATION AND MEASURED

A. 20×20 ARRAY FABRICATION

A prototype of 20 × 20 dual-polarization PUMA has been fabricated in Fig. 10. The surface mount technology (SMT) is used to assemble the resistors and capacitors in the UTLW. Two polarized dipole arms and plates are printed on both sides of Rogers 5880 ($\varepsilon_r = 2.2$) with a thickness of 10 mil. The Rogers 5880 and two layers of substrate (10 mil and 100mil, Rogers 5880LZ) are laminated together using the

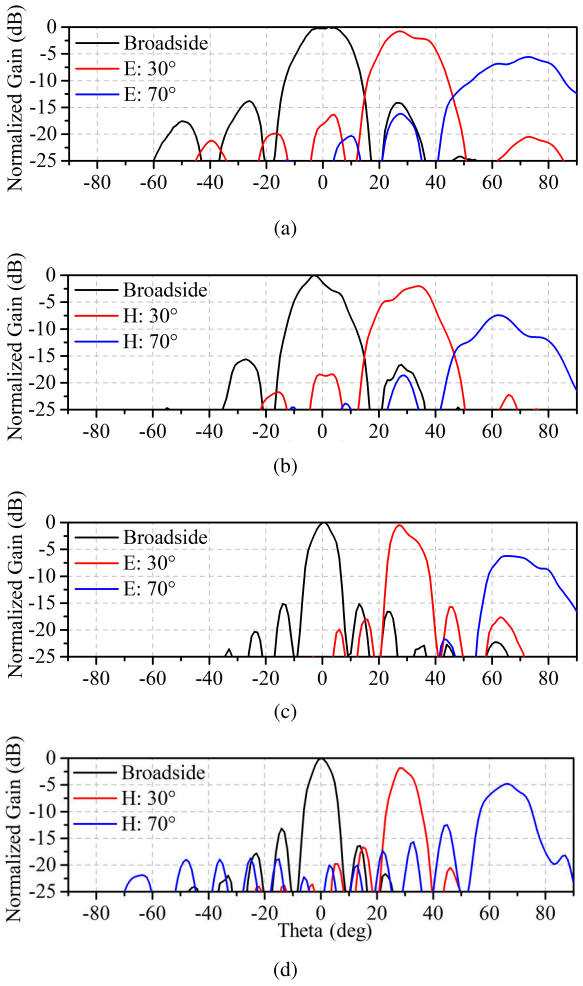

FIGURE 13. Measured radiation pattern of the prototype at 8 GHz and 16 GHz when scanning in E/H-plane. (a) 8 GHz in E-plane. (b) 8 GHz in H-plane. (c) 16 GHz in E-plane. (d) 16 GHz in H-plane.

prepreg layer (3 mil, $\varepsilon_r = 2.8$). The ground plane layer is double-sided copper-clad Rogers 5880 (20 mil), and the copper surfaces on both sides are short circuited by metallized vias. The long inner cores of the mini-sub-miniature push-on connectors (Mini-SMPs) pass through all substrate layers and are welded with dipole arms. The metal plate supports the overall structure at the bottom layer.

B. MEASURED ACTIVE VSWR OF THE PROTOTYPE

The measured active VSWR of the center element is shown in Fig. 11. The measured active VSWR calculated following the equation (6) [20]

$$ActiveS_{nn} = S_{nn} + \sum_{m \neq n} S_{nm} \cdot \frac{a_m}{a_n} \tag{6}$$

where S in equation (6) is the complex ratio of the S parameter. a_m and a_n are complex values of excitations and consist of amplitudes and phases. The main method is to measure the passive reflection coefficient of the reference antenna cell and the mutual coupling of all other antenna cells to the

TABLE 2. Comparison of array performance.

Ref.	Profile	Bandwidth	Scanning	VSWR	Rad. Effic.
[9]	$0.2\lambda_l$	2.25:1 (6.5-14.6 GHz)	$\pm 50°$	≤ 3	88%
[11]	$0.14\lambda_l$	3:1 (7-21 GHz)	$\pm 45°$	≤ 2.8	83%
[12]	$0.08\lambda_l$	6:1 (3.53-21.2 GHz)	$\pm 60°$	≤ 3.8	89%
This work	$0.07\lambda_l$	3:1 (6-18 GHz)	$\pm 70°$	≤ 3	76%

Note: The bandwidth of this work is determined by PUMA scheme. Rad. Effic. means broadside radiation efficiency.

reference antenna cell first, then compensate the scanning phase difference, and finally calculate the active reflection coefficient of the reference antenna cell following equation (6). This measured method need no phase shifter or other RF components, and can accurately obtain the active VSWR of the antenna array. The simulated and measured results indicate that the PUMA with UTLW has excellent impedance matching characteristics under large angle scanning in both E-plane and H-plane.

C. MEASURED RADIATION PATTERN OF THE PROTOTYPE

The measured far-field radiation pattern and realized gain following the unit excitation active element pattern method (UEAEP) [21] is shown in Fig. 12 and Fig. 13. In practice, only the 16×16 elements in the center of the array are excited, and the other elements are regarded as dummy elements. The measured and simulated broadside gain are compared in Fig. 12. In addition, the cross-polarization ratio of the array is less than -18 dB in the whole operating frequency band.

Table 2 compares the performance based on the profile height, bandwidth, scanning angles, active VSWR and broadside radiation efficiency. All antennas in the table are fed by unbalanced lines. Compared with the other schemes, the proposed PUMA with UTLW has the lowest profile height, the largest scanning angles and excellent impedance matching performance.

IV. CONCLUSION

A low-profile and wide-angle scanning PUMA with WAIM is proposed in this paper. Some necessary analysis and derivation are used to predict the complex impedance characteristics of the UTLW. The simulation results of the single-polarized PUMA with UTLW show that the UTLW can replace the WAIM realizing the low-profile characteristics while maintain an excellent performance. Furthermore, a dual-polarized prototype with UTLW is fabricated and measured. The measured results show that the PUMA with UTLW achieves a 3:1 (6-18 GHz) bandwidth with $\pm 70°$ scanning in E/D/H plane. The distance from the top of UTLW to the ground plane is less than $0.07\lambda_l$. In addition, theoretical analysis and simulation show that UTLW has the potential of wider bandwidth, and further work will study reducing profile height of a wider bandwidth antenna array used with UTLW.

REFERENCES

[1] R. W. Kindt and W. R. Pickles, "Ultrawideband all-metal flared-notch array radiator," *IEEE Trans. Antennas Propag.*, vol. 58, no. 11, pp. 3568–3575, Nov. 2010.
[2] J. T. Logan, R. W. Kindt, and M. N. Vouvakis, "A 1.2–12 GHz sliced notch antenna array," *IEEE Trans. Antennas Propag.*, vol. 66, no. 4, pp. 1818–1826, Apr. 2018.
[3] W. Elsallal, J. B. West, J. Wolf, R. Freeman, R. Legge, V. Olen, T. W. Darymple, M. B. Longbrake, and P. E. Buxa, "Charateristics of decade-bandwidth, balanced antipodal vivaldi antenna (BAVA) phased arrays with time-delay beamformer systems," in *Proc. IEEE Int. Symp. Phased Array Syst. Technol.*, Oct. 2013, pp. 111–116.
[4] J. P. Doane, K. Sertel, and J. L. Volakis, "A wideband, wide scanning tightly coupled dipole array with integrated balun (TCDA-IB)," *IEEE Trans. Antennas Propag.*, vol. 61, no. 9, pp. 4538–4548, Sep. 2013.
[5] H. Zhang, S. Yang, S. Xiao, Y. Chen, and S. Qu, "Low-profile, lightweight, ultra-wideband tightly coupled dipole arrays loaded with split rings," *IEEE Trans. Antennas Propag.*, vol. 67, no. 6, pp. 4257–4262, Jun. 2019.
[6] S. S. Holland and M. N. Vouvakis, "The planar ultrawideband modular antenna (PUMA) array," *IEEE Trans. Antennas Propag.*, vol. 60, no. 1, pp. 130–140, Jan. 2012.
[7] R. C. Hansen, "Linear connected arrays [coupled dipole arrays]," *IEEE Antennas Wireless Propag. Lett.*, vol. 3, pp. 154–156, 2004.
[8] D. Cavallo, A. Neto, and G. Gerini, "Analytical description and design of printed dipole arrays for wideband wide-scan applications," *IEEE Trans. Antennas Propag.*, vol. 60, no. 12, pp. 6027–6031, Dec. 2012.
[9] W. H. Syed, D. Cavallo, H. T. Shivamurthy, and A. Neto, "Wideband, wide-scan planar array of connected slots loaded with artificial dielectric superstrates," *IEEE Trans. Antennas Propag.*, vol. 64, no. 2, pp. 543–553, Feb. 2016.
[10] Y. Li, S. Xiao, C.-H. Hu, and Z. Yao, "A low-profile light-weight wideband connected parallel slot array for wide-angle scanning," *IEEE Trans. Antennas Propag.*, vol. 68, no. 2, pp. 813–823, Feb. 2020.
[11] S. S. Holland, D. H. Schaubert, and M. N. Vouvakis, "A 7–21 GHz dual-polarized planar ultrawideband modular antenna (PUMA) array," *IEEE Trans. Antennas Propag.*, vol. 60, no. 10, pp. 4589–4600, Oct. 2012.
[12] J. T. Logan, R. W. Kindt, M. Y. Lee, and M. N. Vouvakis, "A new class of planar ultrawideband modular antenna arrays with improved bandwidth," *IEEE Trans. Antennas Propag.*, vol. 66, no. 2, pp. 692–701, Feb. 2018.
[13] H. Wheeler, "Simple relations derived fom a phased-array antenna made of an infinite current sheet," *IEEE Trans. Antennas Propag.*, vol. AP-13, no. 4, pp. 506–514, Jul. 1965.
[14] H. Zhang, S. Yang, S. Xiao, Y. Chen, S. Qu, and J. Hu, "Ultrawideband phased antenna arrays based on tightly coupled open folded dipoles," *IEEE Antennas Wireless Propag. Lett.*, vol. 18, no. 2, pp. 378–382, Feb. 2019.
[15] J. Zhong, A. Johnson, E. A. Alwan, and J. L. Volakis, "Dual-linear polarized phased array with 9:1 bandwidth and 60° scanning off broadside," *IEEE Trans. Antennas Propag.*, vol. 67, no. 3, pp. 1996–2001, Mar. 2019.
[16] H. A. Wheeler, "The radiation resistance of an antenna in an infinite array or waveguide," *Proc. IRE*, vol. 36, no. 4, pp. 478–487, Apr. 1948.
[17] B. Munk, R. Taylor, T. Durharn, W. Croswell, B. Pigon, R. Boozer, S. Brown, M. Jones, J. Pryor, S. Ortiz, and J. Rawnick, "A low-profile broadband phased array antenna," in *Proc. IEEE Antennas Propag. Soc. Int. Symp.*, vol. 2. Jun. 2003, pp. 448–451.
[18] A. K. Bhattacharyya, "Floquet modal functions," in *Phased Array Antennas: Floquet Analysis, Synthesis, BFNs and Active Array Systems*, 1st ed. Hoboken, NJ, USA: Wiley, 2006, ch. 3.
[19] B. A. Munk, D. S. Janning, R. J. Marheka, J. F. McCann, and S. W. Schneider, "The design of wideband arrays of closely-spaced wire and slot elements," in *Proc. IEEE Antennas Propag. Soc. Int. Symp.*, Jul. 2010, pp. 1–4.
[20] F. B. Gross, *Forntiers in Antennas: Next Generation Design Engineering*, New York, NY USA: McGraw-Hill, 1994, pp. 127–166.
[21] D. M. Pozar, "The active element pattern," *IEEE Trans. Antennas Propag.*, vol. 42, no. 8, pp. 1176–1178, May 1994.

XIN QUAN was born in Henan, China, in 1993. He received the bachelor's degree in electronic information science and technology from the Nanjing University of Aeronautics and Astronautics, Nanjing, China, in 2015. He is currently pursuing the Ph.D. degree in electromagnetic field and microwave technology with Southeast University, Nanjing.

His current research interests include phased-array antennas and base station antennas.

ZHENXIN CAO (Member, IEEE) was born in May 1976. He received the M.S. degree from the Nanjing University of Aeronautics and Astronautics, China, in 2002, and the Ph.D. degree from the School of Information Science and Engineering, Southeast University, China, in 2005.

From 2012 to 2013, he was a Visiting Scholar at North Carolina State University. Since 2005, he has been with the State Key Laboratory of Millimeter Waves, Southeast University, where he is a Professor. His research interests include antenna theory and application.

HUAIMIN ZHOU was born in Shandong, China, in 1999. He received the bachelor's degree in detection guidance and control technology from the Nanjing University of Science and Technology, Nanjing, China, in 2021. He is currently pursuing the master's degree in electromagnetic field and microwave technology with Southeast University, Nanjing.

His current research interest includes tightly coupled dipole antennas.

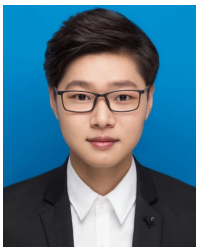

SHENGCHI ZHU was born in Liaoning, China, in 1998. He received the B.S. degree in information engineering from Southeast University, Nanjing, China, in 2020, where he is currently pursuing the Ph.D. degree in electromagnetic field and microwave technology with the State Key Laboratory of Millimeter Waves.

His current research interests include phased-array antennas and frequency selective rasorber.